Energetics of salt-bearing sodalites, $Na_8Al_6Si_6O_{24}X_2$ (X = SO_4, ReO_4, Cl, I): treatment option for pertechnetate-enriched nuclear waste streams

Kristina Lilova[a,#], Eric M. Pierce[b,#], L. Wu[a], Aaron M. Jubb[b], T. Subramani[a], Alexandra Navrotsky[a,*]

[a]Navrotsky Eyring Center for Materials of the Universe, School of Molecular Sciences, Arizona State University, P.O. Box 871604, Tempe, AZ 85287

[b]Environmental Sciences Division, Oak Ridge National Laboratory, P.O. Box 2008, MS: 6038, Oak Ridge, TN 37831

KEYWORDS[1]**:** perrhenate sodalite, enthalpy of formation, ion exchange, radioactive waste

[#]Co-first authors: both contributed equally to this manuscript.

[*]Corresponding Author:
Alexander Navrotsky
Phone: (480) 965-5932
Email: Alexandra.Navrotsky@asu.edu

Abstract

An alternative option for treating anion-enriched reprocessed nuclear waste streams is to immobilize technetium-99 (^{99}Tc, β = 293.7 keV, $t_{1/2}$ = 2.1 × 10^5 years) and other anions in micro- and meso-porous materials. Here we determine the thermodynamic stability of anion bearing sodalites, $Na_8Al_6Si_6O_{24}X_2$ (X = SO_4, ReO_4, Cl, I), to improve our understanding of the driving forces that control framework assembly using high temperature oxide melt solution calorimetry. Raman and FTIR spectroscopy illustrate a strong dependence for vibrational features on anion size and enabled the development of a linear model that predicted the vibrational features for numerous anion bearing sodalites to within ±20 cm^{-1} (i.e., OH, F, Br, ClO_4, NO_3, and MnO_4). The largest negative enthalpy of formation from elements and the lack of structural water demonstrate that the perrhenate sodalite ($Na_8Al_6Si_6O_{24}[ReO_4]_2$), a chemical analogue for pertechnetate sodalite ($Na_8Al_6Si_6O_{24}[TcO_4]_2$), is more thermodynamically stable than all other anion bearing sodalites evaluated. The enthalpies of the reaction between nepheline and the sodium salt, which provides the guest anion species, was negative only for the ReO_4 and NO_3 bearing sodalites. We report for the first time the enthalpy of the ion exchange reactions for different anion bearing sodalites relative to the perrhenate sodalite, which is a key step in gaining the ability to tune sodalite material properties and structure during treatment and the immobilization of ^{99}Tc in the presence of competing anions.

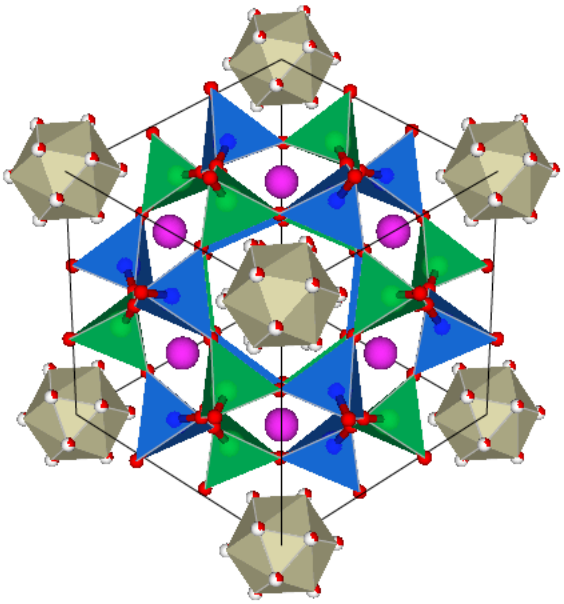

I. Introduction

Micro- and meso-porous solids support a range of industrial uses; including petrochemical cracking, ion exchange for water softening and purification, and gas separation. There is renewed interest in the application of porous solids, such as the sodalite group minerals, for the sequestration, immobilization, and treatment of anion-enriched waste streams which contain long-lived radionuclides (e.g., $^{99}TcO_4^-$, $^{129}I^-$, $^{75}SeO_4^{2-}$) that volatilize during high temperature treatment processes (e.g., vitrification)[1-8].

Feldsphathoid minerals, such as sodalite, have a three-dimensional (3D) porous structure that is composed of alternating TO_4 (T = Al or Si) tetrahedral units that share corner oxygens and form a pore or cavity system that can expand (microporous 2.5 to 20 Å; mesoporous 20 to 500 Å) to encase guest molecules (Br^-, Cl^-, F^-, I^-, OH^-, MnO_4^-, SO_4^{2-}, SeO_4^{2-}, ReO_4^-, TcO_4^-, and WO_4^{2-}) by cooperative changes in the T—O—T bond angles[2-5, 9-14]. Although these solids have been studied for decades, we still lack the ability to tune the material properties and structure during synthesis. The inability to exert control over and direct the symmetry and size of pores, the strength of the active site, and characteristic nature of the material, limits our ability to selectively and efficiently sequester anions during material synthesis and treatment of anion-enriched nuclear waste streams.

Recent studies by Dickson et al.[3-5] suggested that anion selectivity for the β-cage is anion size-dependent. This hypothesis was further explored by conducting experiments to determine the amount of perrhenate (ReO_4^-), a non-radioactive surrogate for pertechnetate (TcO_4^-), incorporated into sodalite in the presence of competing anions ranging in size and charge (e.g., Cl^-, CO_3^{2-}, SO_4^{2-}, MnO_4^-, and WO_4^{2-})[3, 4]. These results illustrated that competitive incorporation of ReO_4^- increased when anions with a similar ionic radius and charge were present in sufficient concentrations.[3] While those studies provide experimental evidence for anion selectivity in sodalites, we still lack a clear understanding of the driving forces that govern framework assembly during synthesis in the presence of competing anions. This is

particularly important for understanding how these structures form and their stability in extreme environments, such as the high radiation environment present in anion-enriched reprocessed nuclear waste streams. The primary objective of the present study is to assess the thermodynamic stability of anion bearing sodalites relative to the enthalpy of formation from nepheline and sodium salt and from the elements. We report, for the first time, the enthalpy of the ion exchange reactions for sodalites containing different anions relative to the perrhenate sodalite ($Na_8Al_6Si_6O_{24}[ReO_4]_2$), which serves as a chemical analogue for pertechnetate sodalite ($Na_8Al_6Si_6O_{24}[TcO_4]_2$).

II. Experimental Methods

Synthesis

The synthesis, particle size, and surface area of the anion bearing sodalites, $Na_8Al_6Si_6O_{24}X_2$ (X = SO_4, ReO_4, Cl, I), used in this study are described in detail elsewhere[14, 15]. A solid state reaction with zeolite 4A, $Na_{12}[(AlO_2)_{12}(SiO_2)_{12}]\bullet H_2O$, was used to synthesize nepheline[16]. Zeolite 4A was placed in 95% Pt-5% Au crucibles and heated in a furnace initially to 1273 K for 6 hours, then to 1323 K for 4 hours, and finally to 1373 K for 4 hours. The synthesized nepheline particles ranged in size from 5 to 264 μm and had a N_2-BET surface area of 1.01 m^2/g.

Characterization

The phase purity and lattice parameters of all compounds were verified by X–ray powder diffraction; the particle size of the anion bearing sodalites was determined using SEM and laser diffraction particle size analyses; the compositions of the samples are checked by electron microprobe and digestion followed by elemental analysis; and the presence and the amount of the structural water was determined by FTIR and thermogravimetry. All characterization techniques and instrumentation were described previously[14, 15]. The Raman spectroscopy, neutron powder diffraction, neutron activation analysis, and the X-ray

absorption spectroscopy measurements for perrhenate sodalite are discussed in Pierce et al.[14].

The X–ray powder diffraction on nepheline was carried on Bruker D8 Advance diffractometer (Cu $K\alpha_1$ wavelength = 1.5406 Å, Cu:40 kV, 40 mA) with a step size of 0.01º and collection time of 40 minutes. FTIR solid–state spectroscopy to check for waters of hydration was performed using Bruker Equinox 55 FTIR spectrometer. The homogeneity and stoichiometry of the nepheline were verified by wavelength dispersive analysis using a Cameca SX–100 electron microprobe with HV of 15 kV, beam current of 2 nA and beam size of 10 μm. The elemental analysis of the nepheline was performed alkaline digestion followed by chemical analysis of the resulting solution.

Raman and infrared spectra of nepheline and the anion bearing sodalites, $Na_8Al_6Si_6O_{24}X_2$ (X = SO_4, ReO_4, Cl, I), were collected on a Renishaw micro-Raman spectrometer (Renishaw Inc.) and Nicolet Magna-760 Fourier transform infrared (FTIR) spectrometer, respectively. The Raman spectrometer is equipped with a 300 mW near-infrared diode laser for excitation at a wavelength of 785-nm. The laser beam was set in position with a 50×, 0.5-numerical aperture Leica microscope objective at a lateral spatial resolution of ~2-mm. A charge-coupled device array detector was used to achieve signal detection from a 1200 groove/mm grating light path controlled by Renishaw WiRE software. Prior to measuring each sample, an instrument performance check was conducted to verify the peak position and intensity using a silicon standard. Infrared spectra were recorded in the 400 – 4000 cm^{-1} at 4 cm^{-1} steps on a FTIR spectrometer equipped with a liquid nitrogen cooled MCT (Mercury-Cadmium-Tellurium) detector. All sample spectra were background corrected by collecting spectra on a clean ZnSe window in air.

Raman and FTIR spectra were fit with a sum of Lorentzian profiles and a linear baseline from 250-1100 cm^{-1} and 600-1300 cm^{-1}, respectively. No parameters were fixed during fitting. A Lorentzian profile was chosen to fit the spectra here considering the inherent Lorentzian nature of the harmonic oscillator model for molecular vibrations[17].

Calorimetry

The low temperature heat capacities for the anion bearing sodalites were measured and reported previously using a Quantum Design Physical Properties Measurement System (PPMS) as described in Schliesser et al.[15]. The standard thermodynamic functions were calculated from these data.

High temperature oxide melt solution calorimetry was performed using a Tian Calvet twin calorimeter as described in Navrotsky[18-20]. In the drop solution calorimetry experiment, samples in the form of pellets (between 4 and 6 mg) were dropped from room temperature (298 K) into the molten lead borate solvent ($2PbO \cdot B_2O_3$) and maintained at the 973 K calorimeter temperature in a platinum crucible. Air was flushed over the solvent at 90 mL/min. The calorimeters were calibrated using the heat content of 5 mg α–Al_2O_3 pellets.

A preliminary furnace test was performed prior to the solution calorimetric measurements for all compounds to assure their complete dissolution in $2PbO \cdot B_2O_3$. During the dissolution, the chlorine and iodine – containing sodium salts and sodalites were checked for a presence of chlorine or iodine vapors above the melt. Hence, the quenched melt was dissolved in diluted nitric acid and the solution was tested for a presence of Cl^- or I^- ions, using $AgNO_3$. White AgCl and pale yellow AgI precipitates were formed, respectively, which verified that Cl^- and I^- anions were not oxidized to Cl_2 and I_2 by the atmospheric O_2 and expelled from the melt. For each sample, the dissolution process started immediately and finished in a minute. After quenching the melt, no undissolved material was found. The qualitative analytical reaction with $AgNO_3$ resulted in a formation of white AgCl and pale yellow AgI precipitates.

Thermogravimetry

A nepheline sample with initial mass of 141.37 mg was heated in air at 973 K for 3 hours with 10 K/min. The final mass after the heating was 141.30 mg, which is within the error of the balance. No

significant weight change was registered, which confirms the FTIR spectroscopy results indicating no water. The details of thermogravimetry on the anion bearing sodalites are published in Pierce et al.[14] and Schliesser et al.[15].

III. Results and Discussion

Characterization

Nepheline was found to be a single phase with hexagonal structure and lattice parameters a = 9.97066 ± 0.001223 Å and c = 8.33555 ± 0.001062 Å. The stoichiometric nepheline has the same structure but with a = 9.978 Å and c = 8.33 Å (PDF card# 35–0424). According to Buerger et al.[21], who studied a natural sample, containing potassium, the reported lattice parameter were larger: a = 10.01 Å and c = 8.405 Å. Tait et al.[22] list different natural samples with lattice parameter between a = 9.985 Å – 10.01 Å; c = 8.3852 Å – 8.405 Å and two synthetics with a = 9.964 Å and c = 8.360 Å and a = 9.968 Å and c = 8.380 Å. In general, the lattice parameters decrease with the Al/Al+Si ratio. All natural samples contain K and Ca as well as vacancies. Authors also provide X–ray data for a natural specimen from a high temperature environment give a = 9.9953 Å and c = 8.3822 Å and microprobe data which indicate composition close to $K_2Na_6Si_8Al_8O_{32}$. Hamilton and Mackenzie[23], suggest a = 9.979 Å, c = 8.331 Å for stoichiometric nepheline and a = 9.968 – 9.971 Å and c = 8.342 –8.351 Å for $NaAlSiO_4$ – SiO_2 solid solutions. For simplicity the solid solution sample here will be called “nepheline”.

The electron microprobe results suggest single nepheline phase with a formula of $Na_{0.90(2)}Al_{0.88(2)}Si_{1.12(2)}O_{4.00(1)}$ which indicates a solid solution with Al/(Al+Si) ratio of 0.44 rather than stoichiometric $NaAlSiO_4$ with Al/(Al+Si) = 0.5. The potassium content in the sample is negligible, ~0.1 at. % which is within the error of the microprobe and will not be considered further. The elemental analysis for nepheline confirms the solid solution stoichiometry from the electron microprobe within the experimental errors. The XRD and composition results for the anion bearing sodalites are discussed in

detail in Pierce et al.[14] and Schliesser et al.[15].

Raman and infrared spectroscopy

Raman and FTIR spectra for the anion bearing sodalites, $Na_8Al_6Si_6O_{24}X_2$ (X = SO_4, ReO_4, Cl, I) are displayed in Fig. 1 at 250-1100 cm^{-1} and 600-1300 cm^{-1}, respectively. The Raman and FTIR spectra for nepheline are consistent with previous results and are provided in the Supporting Information (Fig. SI1). These frequency ranges encompass the bending and stretching vibrations of TO_4 tetrahedra[24-29]. Here we limit our analysis to the major TO_4 tetrahedra symmetric bending [δ-(A1/T2), ~450 cm^{-1}] and symmetric stretching [ν-(A1), ~1000 cm^{-1}] peaks in the Raman spectra and the symmetric stretching [νSS-(TOT)), ~650-750 cm^{-1}] and asymmetric stretching [νAS-(TOT), ~1000 cm^{-1}] peaks in the FTIR spectra. For vibrational spectra of sodalites, splitting of the Raman and infrared active longitudinal optical and transverse optical (LO-TO) phonon modes is known to occur[28]; however, a detailed discussion covering the origin for all observed spectral features is beyond the scope of this study. For both sulfate (SO_4) and perrhenate (ReO_4) containing sodalite [i.e., $Na_8Al_6Si_6O_{24}SO_4$ and $Na_8Al_6Si_6O_{24}(ReO_4)_2$] these frequency ranges also encompass anion vibrational modes including bending, symmetric, and asymmetric stretching from SO_4 and ReO_4 tetrahedra. While the presence of these anionic vibrations does not generally inhibit the analysis of the sodalite vibrational modes, they do complicate an infrared analysis for $Na_8Al_6Si_6O_{24}SO_4$ as the broad νAS-(TOT) peak occurs at a similar frequency (~1100 cm^{-1}) as asymmetric stretching in SO_4 ions.

Since the late 1970s it has been recognized that the vibrational features of sodalites vary with cell parameters, which are strongly influenced by the size of the anion hosted within the sodalite β-cage[24, 30]. These structure – spectra relationships have since been highlighted many times within the literature[25-28, 31-33] and continue to provide insight into sodalite materials with novel compositions[8, 34-36]. While sodalite vibrational features are generally compared directly against cell parameters determined using XRD[24], it is

also possible to relate these features to the ionic radius of the anion for sodalites with identical cation composition. The frequencies for the major Raman and FTIR peaks as a function of the anion radius are shown in Fig. 2 where it is observed that the two major Raman and four major infrared peak frequencies display a strong linear relationship with anion radius (R^2 values all > 0.9).

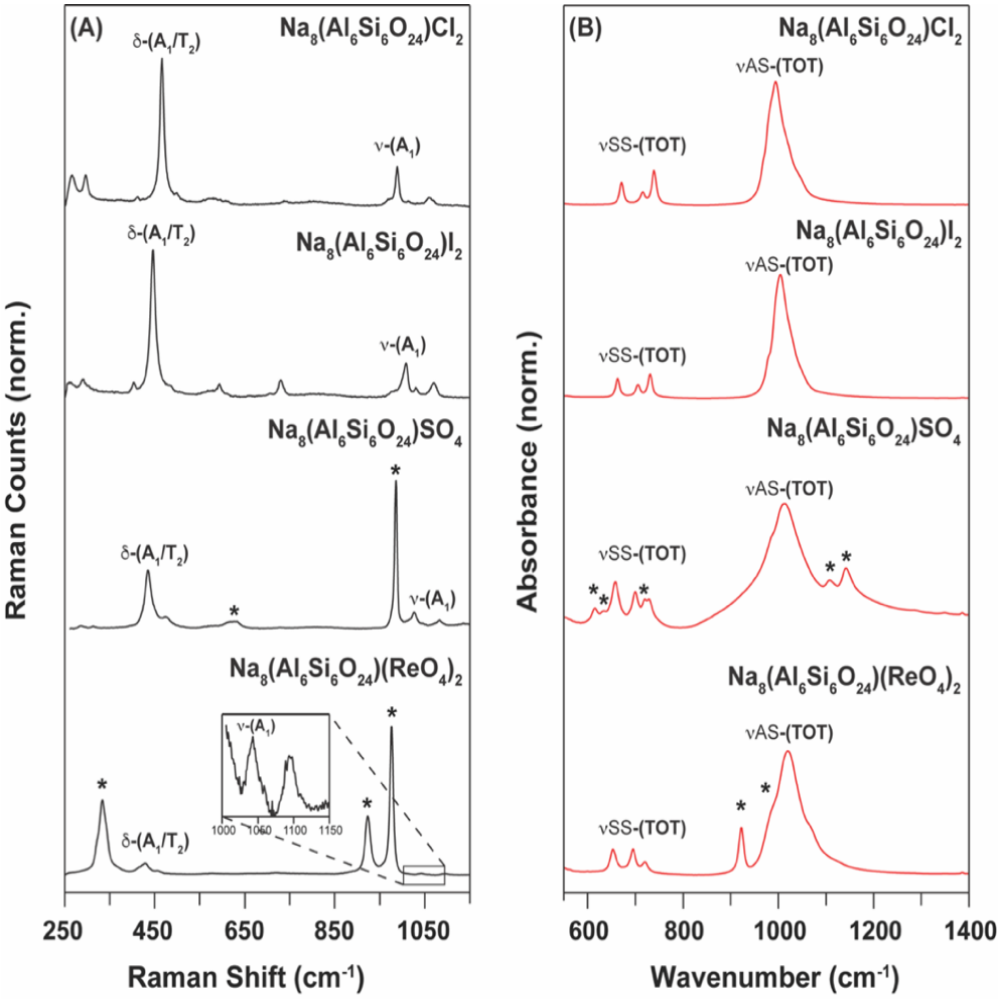

Fig. 1. Vibrational spectra of the anion bearing sodalites under study here. (A) Raman spectra with the TO_4 tetrahedra symmetric bending [δ-(A1/T2), ~450 cm^{-1}] and symmetric stretching [ν-(A1), ~1000 cm^{-1}] peaks labeled. Inset for $Na_8(Al_6Si_6O_{24})(ReO_4)_2$ spectrum highlights ν-(A1) region as response from ReO_4^- vibrations dominate spectral intensity. (B) Fourier transform infrared spectra with three TO_4 tetrahedra symmetric stretching [νSS-(TOT)), ~650-750 cm^{-1}] and one asymmetric stretching [νAS-(TOT), ~1000 cm^{-1}] peaks labeled. Asterisks in (A) and (B) indicate anion vibrational modes for $Na_8(Al_6Si_6O_{24})SO_4$ and $Na_8(Al_6Si_6O_{24})(ReO_4)_2$ samples. All spectra have been baseline corrected, normalized, and scaled vertically for clarity.

The strong dependence of vibrational features on anion size, as exhibited in Fig. 2, is unsurprising as the incorporated anion size will directly influence the resulting β-cage size; i.e., for larger anions T-O bond lengths and T-O-T bond angles will both increase[28]. Using linear empirical relationships, Table 1, between the sodalite vibrational spectra and the respective anion radius it is possible to predict the frequencies for these major spectral peaks for sodalites containing other anions beyond the four measured here. Using the linear models described in Table 1 we can reproduce literature frequencies for Na-sodalites containing OH and Br to within ± 20 cm^{-1} (and typically much better). These results along with predicted values for ClO_4, NO_3, MnO_4, MoO_4, TcO_4, and WO_4 containing Na-sodalites are summarized in Table 2. Larger deviations are observed between the predicted and measured vibrational frequencies for OH-containing sodalite which is attributed to the small radii of OH anion (~50 pm smaller than Cl anion) and so fall far outside of the linear regression model bounds. Nonetheless, the agreement between the predicted and literature values highlighted in

Table **2** demonstrates the degree to which sodalite structural features can be predicted from even a limited number of spectroscopic signatures, and vice versa. Finally, it is important to note that the anionic radii used for the linear regression models were taken from measurements of aqueous hydrated ions[37] and so should represent an upper-bound estimate for the anion radius hosted in the sodalite beta-cages.

Table 1. Linear regressions relating major sodalite vibrational peak frequencies to beta-cage hosted anion radii:

$$\nu_{sodalite} = a + b(r_{anion})$$

where $\nu_{sodalite}$ is the vibrational frequency and r_{anion} is the radius of the anion in picometers taken from Marcus[37].

Linear Regression Coefficients	**Raman Peaks**		**Infrared Peaks**			
	δ-(A1/T2)	**ν-(A1)**	**1: νSS-(TOT)**	**2: νSS-(TOT)**	**3: νSS-(TOT)**	**νAS-(TOT)**
a	556	865	782	762	712	937
b	-0.500	0.677	-0.237	-0.263	-0.228	0.316

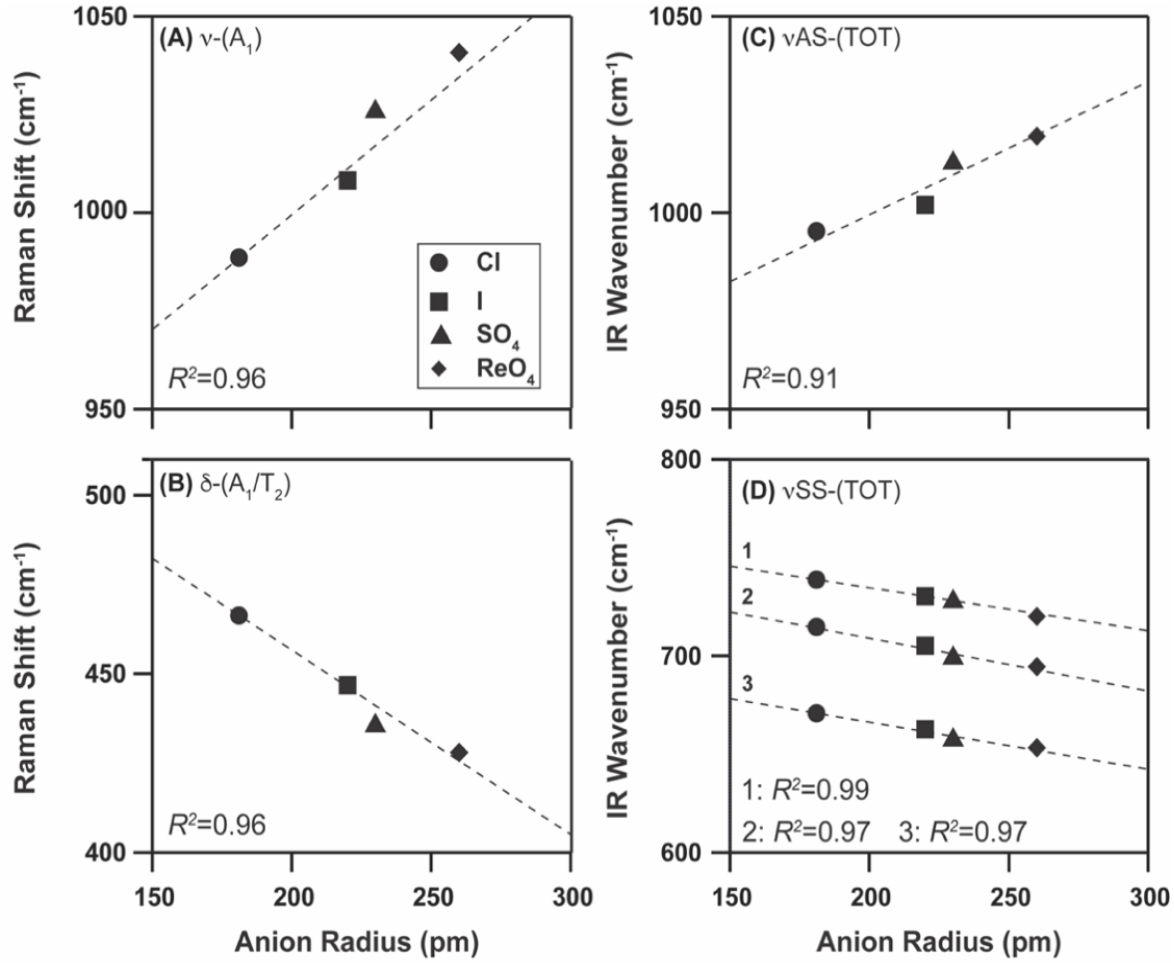

Fig. 2. Dependence of sodalite vibrational peak frequency on anionic radius. (A) Raman ν-(A1) peak; (B) Raman δ-(A1/T2) peak; (C) Infrared νAS-(TOT) peak; and (D) Infrared νSS-(TOT) peaks. Legend is the same for all panels. Dashed lines in each panel represent linear regression fits to the data. Linear regression correlation coefficients for each fit are inset. For (D) linear regression fits and corresponding correlation coefficients are labeled "1", "2", or "3".

Table 2. Predicted frequencies of major Raman and IR Na-sodalite peaks, for a variety of anion-bearing Na sodalites not measured here. For OH and Br containing sodalites absolute differences in wavenumbers between predicted (bold) and literature peak frequencies (italics) are provided.

		Raman Peaks		Infrared Peaks			
Anion	**[a]Radius (pm)**	**δ-(A1/T2) (cm^{-1})**	**ν-(A1) (cm^{-1})**	**1: νSS-(TOT) (cm^{-1})**	**2: νSS-(TOT) (cm^{-1})**	**3: νSS-(TOT) (cm^{-1})**	**νAS-(TOT) (cm^{-1})**
OH	133	**490**	**955**	**750**	**727**	**682**	**979**
		-	-	*20[b]*	*15[b]*	*25[b]*	*14[b]*
F	133	**490**	**955**	**750**	**727**	**682**	**979**
NO_3	179	**467**	**986**	**740**	**715**	**671**	**994**
Br	196	**458**	**998**	**736**	**710**	**667**	**999**
		10[d]	*24[d]*	*2[b], 4[c], 2[d]*	*4[b], 2[c]*	*2[b], 3[c], 5[d]*	*4[b], 14[c], 31[d]*
MnO_4	240	**436**	**1027**	**725**	**699**	**657**	**1013**
ClO_4	250	**431**	**1034**	**722**	**696**	**655**	**1016**
TcO_4	252	**430**	**1036**	**722**	**696**	**655**	**1017**
MoO_4	270	**421**	**1048**	**718**	**691**	**650**	**1022**
WO_4	279	**417**	**1054**	**716**	**689**	**648**	**1025**

[a]Ionic radius values from Marcus[37].
[b]Godber et al.[26]
[c]Taylor, D.[30]
[d]Mofrad et al.[29]

Thermogravimetry

Thermogravimetry was performed on all samples to determine the presence or absence of absorbed or structural water. The initial hydrated SO_4-sodalite (i.e., nosean, $Na_8[Al_6Si_6O_{24}](SO_4)\cdot xH_2O$), containing potentially both adsorbed and structural water in the sample was heated in air at 973 K for 12 hours. A weight loss of 3.03 wt. % was registered. The water (both surface and structural) as well as the sulfate in the initial and dehydrated samples was verified by FTIR spectroscopy. Additional heating at 1173 K for another 12 hours was performed with no weight change and at 1273 K for six hours with 3.60 wt % weight loss, giving 6.63 wt. % in total. The FTIR analysis of the sample after the final heating indicated no absorption bands which can be assigned to molecular water, OH group or surface–adsorbed carbonate,

with the sulfate bands still present. Considering that between the three heating cycles, the sample was exposed to air for prolonged times, additional water was adsorbed on the surface, which increased the total weight loss. In order to verify that no structural changes occurred, XRD was performed on the material after heating to 1273 K and the lattice parameter decreased to within error (9.08901 ± 0.000329 Å), likely due to the removal of the structural water[38]. According to Hassan and Grundy[39], for the stoichiometric structure $Na_8[Al_6Si_6O_{24}](SO_4)\cdot H_2O$, a = 9.084 Å and it depends on the size of $[Na_4SO_4]^{2+}$ and $[Na_4.H_2O]^{4+}$ clusters. Using the thermogravimetry in lead borate solvent to determine the water content of SO_4-sodalite resulted in weight loss of 4.80 wt.% which corresponds to 2.79 mol H_2O. Lower water content than previously obtained confirms the assumption that more water (1.83 wt.%) was adsorbed between the three heating cycles. Additionally, the error of each measurement (estimated to be around 1 wt. % for each measurement) increased accordingly with the number of cycles.

The thermogravimetry of dry chloride and iodide at 1073 K resulted in partial decomposition and loss of Cl_2 and I_2. Using lead borate solvent gave a weight loss of 12 and 10 wt. % or approximately 7.33 and 6.77 mol H_2O, respectively. No vapors above the melt were noticed during the experiment. No weight change was registered for nepheline and perrhenate sodalite, which confirms the lack of water bands observed in the FTIR results for this sample.

Calorimetry

The results from the low temperature heat capacity measurements of the sodalites are published and discussed in Schliesser et al.[15]. Oxide melt solution calorimetry is discussed here.

The drop solution enthalpies of all compounds and the enthalpies of formation from components and from elements are shown in the Table 3. The enthalpies of formation are calculated from the drop solution enthalpies, corrected for the water content in order to be able to compare the stability of the hydrated and anhydrous feldspathoids. All results are calculated for the actual stoichiometry. SO_4-sodalite

($Na_{7.98}Al_6Si_{6.06}O_{24}S_{1.02}O_4 \cdot 2.79H_2O$) is the only sample in this study that dehydrated by annealing without decomposing. The enthalpy of hydration is calculated as 74.90 ± 12.15 kJ/mol per mole water, which is similar to Moloy et al.[40] values for Na_8-hydrosodalites and it is within the experimental error of the heat effect of liquid water 70.2 ± 2.7 kJ/mol[41]. Since all anion bearing sodalites in Table 3 are close to ideal Na_8 structure, and the enthalpies of hydration of the individual compounds are not known, we used the effect of the liquid water to correct the drop solution enthalpies.

The enthalpy of formation from oxides of $Na_{0.90}Al_{0.88}Si_{1.12}O_4$ is calculated and compared with the values for stoichiometric nepheline obtained from literature sources[42-44] and shown in Table 3 and Fig. 3. These values were found to be less negative. The enthalpies of formation from oxides of cristobalite, $Na_{0.90}Al_{0.88}Si_{1.12}O_{4.00}$ solid solution and stoichiometric nepheline points, situated on a straight line are shown in Fig. 3.

The effect of the tetragonal – hexagonal transition between the two end members is not apparent in the drop solution enthalpies (hence in the enthalpies of formation) and the cristobalite – nepheline solid solution behavior appears to be ideal. Substituting silicon by aluminum in the Si–O tetrahedra plus sodium outside the framework results in more negative heats of formation, as seen before for many other materials.[45]

Table 3. Drop solution enthalpies corrected for water, the enthalpies of formation from components, nepheline and components, and from elements. The enthalpies of formation from elements of the component oxides, sodium salts, and anions are taken from Robie and Hemingway[46], Glushko[47], or calculated from FactSage[48].

Compound	ΔH_{ds}, kJ/mol dehydrated	$\Delta H_{f,comp}$, kJ/mol	$\Delta H_{f,neph,comp}$, kJ/mol	$\Delta H_{f,el}$, kJ/mol
$Na_{0.90}Al_{0.88}Si_{1.12}O$	154.5±1.59	–113.55±2.02		–2057.50±2.38
$NaAlSiO_4$	164.92±0.59[a] 167.50±4.10[b] 169.40±0.65[c]	–127.92±1.86 –130.26±4.26 –132.41±1.34		–2067.92±1.87 –2070.50±4.47 –2072.40±1.89
$Na_{7.98}Al_6Si_{6.06}O_{24}S_{1.02}O_4 \cdot 2.79H_2O$	1137.29±9.34	-718.68±8.76[d]	75.73±10.01	–13842.20±13.80
$Na_8Al_6Si_6O_{24}(ReO_4)_2$	1292.07±8.07[d]	–814.02±10.68[d]	–22.57±9.03	–14624.70±13.12
$Na_{8.04}Al_{6.06}Si5.94O_{24}Cl_{1.92} \cdot 7.33H_2O$	944.38±13.01	–604.21±14.87	198.60±13.62	–13149.73±16.63
$Na_{7.64}Al_6Si_6O_{24}I_{1.64} \cdot 6.77H_2O$	846.88± 4.72	–583.61±11.11	211.74±9.33	–12762.68±13.33
$Na_{8.072}Al_{6.055}Si_{5.945}O_{24}(NO_3)_{1.320}(CO_3)_{0.348} \cdot 2.5H_2O$	1546.49±11.12[h]	–819.68± 13.84	-22.91±5.82	–13578.73±15.61
$Na_{8.28}Al_{5.93}Si_{6.07}O_{24}(OH)_{0.49}(CO_3)_{0.93} \cdot 3.64H_2O$	1107.10±50.00[i]	–651.69±57.71		–13669.79±51.04
$Na_{7.82}Al_{5.98}Si_{6.02}O_{24}(OH)_{1.84}$	10009.3±12.4[j]	–830.30±13.3[j]		–13181.7 ±15.1[j]
Na_2O	–112.86±0.97[e]			–414.80±0.30
Al_2O_3	107.45±0.76[f]			–1675.70±1.30
SiO_2	39.70±1.00[g]			–910.70±1.00
Na_2SO_4	196.62±1.10			–1387.80±0.40
$NaReO_4$	126.55±0.55			–1036.00±1.00
NaCl	63.29± 0.88			–411.10±1.00
NaI	25.74± 0.76			–287.90±1.00
SO_4^{2-}				–907.5±0.1
ReO_4^-				–803.33±3.77
Cl^-				–167.10±0.1
I^-				–56.80±0.1
NO_3^-				–206.90±0.4
CO_3^{2-}				-675.20±0.1
OH^-				-230.0±0.1

[a]Hlabse and Kleppa[42]
[b]Akaogi et al.[43]
[c]Navrotsky et al.[44]
[d]Pierce et al.[14]
[e]average drop solution enthalpy from Fialips et al.[49], Kiseleva et al.[50, 51]
[f]drop solution enthalpy of Al_2O_3 which is an average of the values measured over 5 years in The Peter A. Rock Thermochemistry Laboratory
[g]average drop solution enthalpy from Kiseleva et al.[51], Chai and Navrotsky[52], and Trofymluk et al.[53]
[h]Liu et al.[54]
[i]Kurdakova et al.[55]
[j]Moloy et al[40]

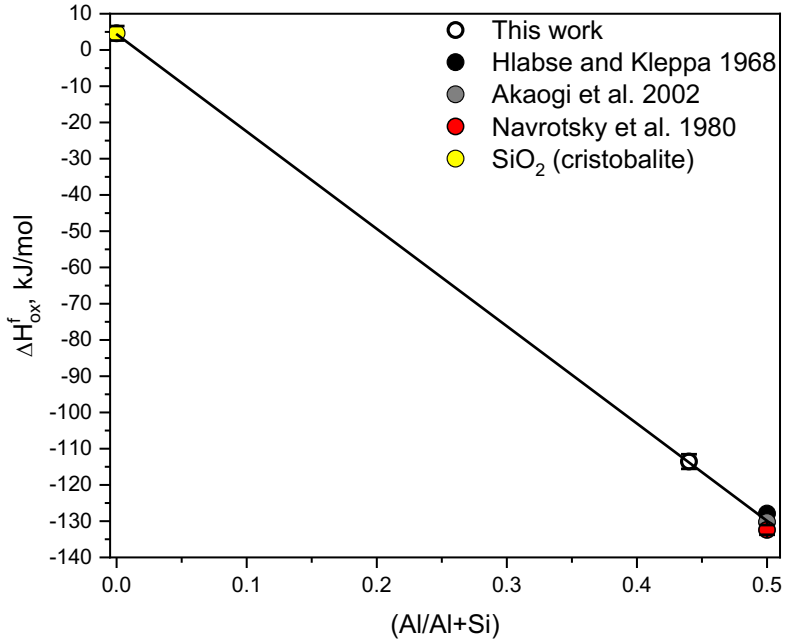

Fig. 3. Enthalpies of formation of cristobalite, the solid solution and nepheline. The empty circle indicates the result for non–stoichiometric nepheline, the black, grey and red circles represent the enthalpies of formation, calculated from Hlabse and Kleppa[42], Akaogi et al.[43], and Navrotsky et al.[44], respectively. The yellow circle is the enthalpy of formation of cristobalite end–member from quartz.

Hlabse and Kleppa[42], Akaogi et al.[43], and Navrotsky et al.[44] state that their samples were characterized by XRD and found to be single phase nepheline. None of these studies reported analyzed chemical compositions and the samples used were assumed to be stoichiometric. The difference in the enthalpy of formation for nepheline between previous measurements and the data collected in this study, is due to differences in composition and not a result of structural changes or impurities (phases or elements). The nepheline sample used in this study is nonstoichiometric (Al/(Al+Si)) < 0.5 as evident by the microprobe and elemental analysis which suggest the ratio Al/Al+Si is 0.44 and 0.435, respectively, instead of 0.5.

The thermodynamic cycles used to calculate the enthalpy of formation of nepheline from oxides and elements and of the sodalites from elements are shown in Table 4 and 5, respectively. The thermodynamic

cycle used to calculate the enthalpy of formation of the sodalites from components is published in Pierce et al.[14]. The perrhenate sodalite appears to be the most thermodynamically stable with respect to the enthalpy of formation from elements. The mixed NO_3/CO_3 cancrinite (Table 3) shows a similar enthalpy of formation from components (oxides and sodium salts) to the perrhenate sodalite within experimental error. It should be noted that the NO_3 and CO_3 cancrinites are mixed anion sodalites, e.g. solid solution between NO_3, CO_3, and OH end members with an unknown mixing enthalpy, which could potentially contribute to the total energetics of the compound.

Additionally, the perrhenate sodalite is the only compound lacking structural water, which is known to help stabilize the structure. The iodide and the chloride sodalites contain the largest amount of structural water in comparison to the other aluminosilicates (Table 3) and have the least exothermic heats of formation from components. The correlation of the enthalpy of formation with the water content indicates that the energetics of the sodalite is a function of the combination of all interactions between the ions and molecules within the structure.

Table 4. Thermodynamic cycles used to calculate the enthalpy of formation of nepheline (solid solution) from oxides and elements.

Reaction number and reaction	Enthalpy of the reaction (kJ/mol)
$Na_{0.90}Al_{0.88}Si_{1.12}O_{4.00}$(s, 298 K) → 0.45$Na_2O$ (soln, 975K) + 0.44Al_2O_3(soln, 975K) + 1.12SiO_2 (soln, 975K)	ΔH_1[a]
Na_2O (s, 298 K) → Na_2O (soln, 975K)	ΔH_2[b]
α–Al_2O_3 (s, 298 K) → Al_2O_3 (soln, 975K)	ΔH_3[c]
SiO_2 (s, 298 K) → SiO_2 (soln, 975K)	ΔH_4[d]
0.45Na_2O (s, 298 K) + 0.44Al_2O_3(s, 298 K) + 1.12SiO_2 (s, 298 K) → $Na_{0.90}Al_{0.88}Si_{1.12}O_{4.00}$ (s, 298 K)	ΔH_5
$\Delta H_5 = \Delta H_{f,ox} = -\Delta H_1 + 0.45\Delta H_2 + 0.44\Delta H_3 + 1.12\Delta H_4$	

Table 5. Thermodynamic cycles used to calculate the enthalpy of formation of a compound $Na_aAl_bSi_cX_xO_{24}$ where X is SO_4, Cl, I, ReO_4, from elements. The numerical values are shown in Table 3.

Reaction	Enthalpy of the reaction (kJ/mol)
$Na_aAl_bSi_cX_xO_{24}$ (s, 298 K) → (a–x)Na_2O (soln, 973K) + xNaX (soln, 973K) + b/2Al_2O_3(soln, 973K) + cSiO_2 (soln, 973K)	ΔH_1
Na_2O (s, 298 K) → Na_2O (soln, 973K)	ΔH_2
α–Al_2O_3 (s, 298 K) → Al_2O_3 (soln, 973K)	ΔH_3
SiO_2 (s, 298 K) → SiO_2 (soln, 973K)	ΔH_4
NaX (s, 298 K) → NaX_4 (soln, 973 K)	ΔH_5
2Na (s, 298 K) + O_2 (g, 298 K) → Na_2O (s, 298 K)	ΔH_7
2Al (s, 298 K) + 1.5O_2 (g, 298 K) → Al_2O_3 (s, 298 K)	ΔH_8
Si (s, 298 K) + O_2 (g, 298 K) → SiO_2 (s, 298 K)	ΔH_9
Na (s, 298 K) + X (g, 298 K) + 2O_2 → NaX (s, 298 K)	ΔH_{10}
aNa (s, 298 K) + bAl (s, 298 K) + cSi (s, 298 K) + xX (s, 298 K) + 16O_2 (g, 298 K) → $Na_aAl_bSi_cX_xO_{24}$ (s, 298 K)	ΔH_{11}
$\Delta H_{11} = \Delta H_{f,el} = -\Delta H_1 + (a-x)\Delta H_2 + b/2\Delta H_3 + c\Delta H_4 + x\Delta H_5 + (a-x)\Delta H_7 + b/2\Delta H_8 + c\Delta H_9 + x\Delta H_{10}$	

The enthalpies of formation from the corresponding sodium salt and nepheline can be calculated according to the equation:

$$NaAlSiO_4 + xNaX = Na_8Al_6Si_6X_xO_{24} \text{ where X} = SO_4, \text{ I, Cl, } ReO_4, CO_3, \text{ and } NO_3$$

For stoichiometric nepheline, the value 169.40 ± 0.65 (Navrotsky et al.[44]) was used (Table 3). All compounds appear metastable (the enthalpy of the reaction is positive) with respect to nepheline and sodium salt except for the perrhenate and the nitrate/carbonate sodalites. The sodium "salt" behavior would be different than that of the bulk one depending on the confinement of the guest species as observed by Liu et al.[54].

Enthalpy of exchange reactions

During the treatment and immobilization of the nuclear waste, ^{99}Tc can compete for the sodalite β-cage with other anions as NO_3^-, SO_4^{2-}, Cl^-, I^-, OH^-. Using the perrhenate sodalite as an analogue for pertechnetate sodalite, the enthalpies of the exchange reactions were calculated using the data in Table 3.

$$Na_8Al_6Si_6O_{24}(ReO_4)_2 + xX^- \rightarrow Na_8Al_6Si_6O_{24}X_x + 2ReO_4^- \ (X = SO_4, CO_3, NO_3, Cl, I, OH)$$

For the species with mixed guest anions such as $Na_{8.072}Al_{6.055}Si_{5.945}O_{24}(NO_3)_{1.32}(CO_3)_{0.348}$, the following reaction was used:

$$Na_8Al_6Si_6O_{24}(ReO_4)_2 + xX^- + yY^- \rightarrow Na_8Al_6Si_6O_{24}X_xY_y + 2ReO_4^-$$

where X_1 and X_2 are CO_3, NO_3, and OH

Table 6. Enthalpies of exchange of perrhenate sodalite and $Na_8Al_6Si_6O_{24}X_2$ (X = SO_4, NO_3, CO_3, Cl, I, OH)

Compound	ΔH_{ex}, kJ/mol
$Na_8Al_6Si_6O_{24}SO_4$	83.34 ± 19.10
$Na_{8.072}Al_{6.055}Si_{5.945}O_{24}(NO_3)_{1.32}(CO_3)_{0.348}$	–52.61 ± 20.37
$Na_{8.28}Al_{5.93}Si_{6.07}O_{24}(OH)_{0.49}(CO_3)_{0.93}$	–23.82 ± 52.69
$Na_{7.82}Al_{5.98}Si_{6.02}O_{24}(OH)_{1.84}$	37.39 ± 20.66
$Na_8Al_6Si_6O_{24}Cl_2$	202.51 ± 21.15
$Na_{7.64}Al_{6.02}Si_{5.95}O_{24}I_{1.64}$	348.51 ± 18.67

Except for the nitrate and carbonate anions, the exchange enthalpies of the other reactions are positive, and suggest such exchange would not be favored (Table 6). These results support the findings of Dickson et al.[5] who showed a larger preference for NO_3 than ReO_4 in the sodalites when the nitrate anion concentration is above 0.9 mole fraction in the mixture.

IV. Implications

The newly obtained data provide valuable information about the guest anion – stability relationship in sodalites. The perrhenate sodalite, which is a chemical analogue for pertechnetate sodalite, is the most thermodynamically stable phase with respect to the enthalpy of formation from elements. The enthalpies

of formation from nepheline and sodium salt of the perrhenate and the nitrate sodalites are negative and within the experimental error of each other; while all other sodalites appear metastable (i.e., the enthalpies of formation from nepheline plus sodium salt are positive). The enthalpies of ion exchange reactions indicate that pertechnetate sodalite, $Na_8Al_6Si_6O_{24}(TcO_4)_2$, will only form after removal of the majority of the nitrate, carbonate, nitrite, and possibly other anions with smaller ionic radii present in reprocessed nuclear waste streams. While sodalites can serve as an alternative treatment and immobilization option for anion-enriched reprocessed nuclear waste streams, the ability to maximize the formation of pertechnetate sodalite in the presence of competing anions will require additional data to assess the potential for the formation of mixed-anion sodalites during treatment.

V. Acknowledgements

We would like to thank David M. Missimer and Feng He for their support at different stages of the research highlighted. Portions of this research were supported by the Subsurface Biogeochemical Research Program under the US Department of Energy (DOE) Office of Biological and Environmental Research and Tank Waste Management Technology Development Program under the Office of Environmental Management. Oak Ridge National Laboratory is managed by UT-Battelle, LLC, for DOE under contract DE-AC05-00OR22725. The calorimetric studies were done several years ago at UC Davis and data analysis were supported at UC Davis by Tank Waste Management Technology Development Program under the Office of Environmental Management while the data analysis and manuscript preparation were supported by Arizona State University.

References

1. Gin, S.; Abdelouas, A.; Criscenti, L. J.; Ebert, W. L.; Ferrand, K.; Geisler, T.; Harrison, M. T.; Inagaki, Y.; Mitsui, S.; Mueller, K. T.; Marra, J. C.; Pantano, C. G.; Pierce, E. M.; Ryan, J. V.; Schofield, J. M.; Steefel, C. I.; Vienna, J. D., An International Initiative on Long-Term Behavior of High-Level Nuclear Waste Glass. *Materials Today* **2013,** *16*, (6), 243-248.

2. Pierce, E. M.; Lukens, W. W.; Fitts, J. P.; Jantzen, C. M.; Tang, G., Experimental determination of the speciation, partitioning, and release of perrhenate as a chemical surrogate for pertechnetate from a sodalite-bearing multiphase ceramic waste form. *Applied Geochemistry* **2014,** *42*, 47-59, DOI: 10.1016/j.apgeochem.2013.12.017.

3. Dickson, J. O.; Harsh, J. B.; Lukens, W. W.; Pierce, E. M., Perrhenate incorporation into binary mixed sodalites: The role of anion size and implications for technetium-99 sequestration. *Chemical Geology* **2015,** *395*, 138-143, DOI: 10.1016/j.chemgeo.2014.12.009.

4. Dickson, J. O.; Harsh, J. B.; Flury, M.; Pierce, E. M., Immobilization and exchange of perrhenate in sodalite and cancrinite. *Microporous and Mesoporous Materials* **2015,** *214*, 115-120, DOI: 10.1016/j.micromeso.2015.05.011.

5. Dickson, J. O.; Harsh, J. B.; Flury, M.; Lukens, W. W.; Pierce, E. M., Competitive Incorporation of Perrhenate and Nitrate in Sodalite. *Environmental Science and Technology* **2014,** *48*, 12851-12857, DOI:

6. Neeway, J. J.; Qafoku, N. P.; Williams, B. D.; Snyder, M. M. V.; Brown, C. F.; Pierce, E. M., Evidence of technetium and iodine release from a sodalite-bearing ceramic waste form. *Applied Geochemistry* **2016,** *66*, 210-218, DOI:

7. Neeway, J. J.; Qafoku, N. P.; Williams, B. D.; Rod, K.; Bowden, M. E.; Brown, C. F.; Pierce, E. M., Performance of the Fluidized Bed Steam Reforming product under hydraulically unsaturated conditions. *Journal of Environmental Radioactivity* **2013,** *131*, 119-128, DOI:

8. Mattigod, S. V.; McGrail, B. P.; McCready, D. E.; Wang, L.; Parker, K. E.; Young, J. S., Synthesis and structure of perrhenate sodalite. *Microporous and Mesoporous Materials* **2006,** *91*, (1-3), 139-144, DOI:

9. Brenchley, M. E.; Weller, M. T., Synthesis and Structruer of M8[AlSiO4]6 (XO4)2, M = Na, Li, K; X = Cl, Mn Sodalites. *Zeolites* **1994,** *14*, 1994, DOI:

10. Depmeier, W., The sodalite family—A simple but versatile framework structure. In *Micro- and Mesoporous Mineral Phases*, Ferraris, G.; Merlino, S., Eds. Mineralogical Society of America/Geochemical Society: Washington, DC, 2005; Vol. 57, pp 203–235, DOI:

11. Trill, H.; Eckert, H.; Srdanov, V., Mixed halide sodalite solid solution system. Hydrothermal synthesis and structural characterization by solid state NMR. *J. Phys. Chem. B* **2003,** *107*, 8779–8788, DOI:

12. Trill, H. Sodalite Solid Solution System. Synthesis, Topotactic Transformations, and Investigation of Framewok-Guest and Guest-Guest Interactions. Westfalische Wilhelms Universitat, Munster, 2002.

13. Trill, H.; Eckert, H.; Srdanov, V., Topotactic transformations of sodalite cages: Synthesis and NMR study of mixed salt-free and salt-bearing sodalites. *Journal of the American Chemical Society* **2002,** *124*, 8361–8370, DOI:

14. Pierce, E. M.; Lilova, K.; Missimer, D. M.; Lukens, W. W.; Wu, L.; Fitts, J.; Rawn, C.; Huq, A.; Leonard, D. N.; Eskelsen, J. R.; B, F. W.; Jantzen, C. M.; Navrotsky, A., Structure and Thermochemistry of Perrhenate Sodalite and Mixed Guest Perrhenate/Pertechnetate Sodalite. *Environ Sci Technol* **2017,** *51*, (2), 997-1006, DOI:

15. Schliesser, J.; Lilova, K.; Pierce, E. M.; Wu, L. L.; Missimer, D. M.; Woodfield, B. F.; Navrotsky, A., Low temperature heat capacity and thermodynamic functions of anion bearing sodalites Na8Al6Si6O24X2 (X = SO4, ReO4, Cl, I). *J Chem Thermodyn* **2017,** *114*, 14-24, DOI:

16. Demitrijevic, R.; Dondur, V.; Vulic, P.; Markovic, S.; Macura, S., Structural characterization of pure Na-nephelines synthesized by zeolite conversion route. *Journal of Physics and Chemistry of Solids* **2004,** *65*, 1623-1633, DOI:

17. Meier, R. J., On art and science in curve-fitting vibrational spectra. *Vib Spectrosc* **2005,** *39*, (2), 266-269, DOI:

18. Navrotsky, A., Progress and New Directions in High-Temperature Calorimetry. *Phys. Chem. Miner.* **1977,** *2*, (1-2), 89-104, DOI:

19. Navrotsky, A., Progress and new directions in high temperature calorimetry revisited. *Phys. Chem. Miner.* **1997,** *24*, (3), 222-241, DOI:

20. Navrotsky, A., Progress and New Directions in Calorimetry: A 2014 Perspective. *Journal of the American Ceramic Society* **2014,** *97*, (11), 3349-3359, DOI:

21. Buerger, M. J.; Klein, G. E.; Donnay, G., Determination of the crystal structure of nepheline. *American Mineralogist* **1954,** *39*, 805-818, DOI:

22. Tait, K. T.; Sokolova, E.; Hawthorne, F. C., The crystal chemistry of nepheline. *Canadian Mineralogist* **2002,** *41*, (1), 61-70, DOI:

23. Hamilton, D. L.; Mackenzie, W. S., Nepheline Solid Solution in the System NaAlSiO4–KAlSiO4–SiO2. *Journal of Petrology* **1960,** *1*, 56-72, DOI:

24. Henderson, C. M. B.; Taylor, D., Infrared spectra of anhydrous members of the sodalite family. *Spectrochimica Acta Part A: Molecular Spectroscopy* **1977,** *33*, (3-4), 283-290, DOI:

25. Ariai, J.; Smith, S. R. P., The Raman spectrum and analysis of phonon modes in sodalite. *Journal of Physics C: Solid State Physics* **1981,** *14*, (8), 1193-1202, DOI:

26. Godber, J.; Ozin, G. A., Fourier Transform Far-Infrared Spectroscopic Study of Cation and Anion Dynamics in M,X-Sodalites, Where M = Li, Na, K, Rb, Ca; X = CI-, Br-, I-, ClO4-, OH. *Journal of Physical Chemistry* **1988,** *92*, (17), 4980-4987.

27. de Man, A. J. M.; van Santen, R. A., The relation between zeolite framework structure and vibrational spectra. *Zeolites* **1992,** *12*, (3), 269-279, DOI:

28. Creighton, J. A.; Deckman, H. W.; Newsam, J. M., Computer simulation and interpretation of the infrared and Raman spectra of sodalite frameworks. *Journal of Physical Chemistry* **1994,** *98*, (2), 448-459, DOI:

29. Mofrad, A. M.; Peixoto, C.; Blumeyer, J.; Liu, J.; Hunt, H. K.; Hammond, K. D., Vibrational Spectroscopy of Sodalite: Theory and Experiments. *Journal of Physical Chemistry C* **2018,** *122*, 24765-24779, DOI:

30. Taylor, D., Cell Parameter Correlations in the Aluminosilicate-Sodalites. *Contributions to Mineralogy and Petrology* **1975,** *51*, (1), 39-47, DOI:

31. Johnson, G. M.; Mead, P. J.; Weller, M. T., Structural trends in the sodalite family. *Physical Chemistry Chemical Physics* **1999,** *1*, 3709-3714.

32. Fischer, R. X.; Baur, W. H., Symmetry relationships of sodalite (SOD) type crystal structures. *Zeitschrift Für Kristallographie - Crystalline Materials* **2009,** *224*, (4).

33. Mikula, A.; Król, M.; Koleżyński, A., The influence of the long-range order on the vibrational spectra of structures based on sodalite cage. *Spectrochimica Acta Part A: Molecular and Biomolecular Spectroscopy* **2015,** *144*, (273-280).

34. McCready, D. E.; Mattigod, S. V.; Young, J. S.; McGrail, B. P., X-ray powder diffraction data for Na8(AlSiO4)6(ReO4)2. *International Center for Diffraction Data: Advances in X-ray Analysis* **2004,** *47*, 297-302.

35. Gesing, T., Structure and Properties of Tecto-Gallosilicates II. Sodium Chloride, Bromide and Iodide Sodalites. *Zeitschrift Für Kristallographie* **2006,** *222*, (6), 289-296.

36. Schneider, A. G.; Bredow, T.; Schomborg, L.; Rüscher, C. H., Structure and IR Vibrational Spectra of Na8[AlSiO4]6(BH4)2: Comparison of Theory and Experiment. *Journal of Physical Chemistry A* **2014,** *118*, (34), 7066-7073.

37. Marcus, Y., Thermodynamics of solvation of ions. Part 5 - Gibbs free energy of hydration t 298. *Journal of the Chemical Society Faraday Transactions* **1991,** *87*, 2995-2999.

38. Taylor, D., The sodalite group of minerals. *Contributions to Mineralogy and Petrology* **1967,** *16*, 172-188.

39. Hassan, I.; Grundy, H. D., The structure of nosean, ideally Na8[Al6Si6O24]SO4.H2O. *Canadian Mineralogist* **1989,** *27*, 165-172.

40. Moloy, E. C.; Liu, Q.; Navrotsky, A., Formation and hydration enthalpies of the hydrosodalite family of materials. *Microporous and Mesoporous Materials* **2006,** *88*, (1-3), 283-292.

41. Navrotsky, A.; Rapp, R. P.; Smelik, E.; Burnley, P.; Circone, S.; Chai, L.; Bose, K., The behavior of H2O and CO2 in high-temperature lead borate solution calorimetry of volatile-bearing phases. *American Mineralogist* **1994,** *79*, 1099-1109.

42. Hlabse, T.; Kleppa, O., The thermochemistry of jadeite. *American Mineralogist* **1968,** *53*, 1281-1292.

43. Akaogi, M.; Tanaka, A.; Kobayashi, M.; Fukushima, N.; Suzuki, T., High-pressure transformations in NaAlSiO4 and thermodynamic properties of jadeite, nepheline, and calcium ferrite-type phase. *Physics of the Earth and Planetary Interiors* **2002,** *130*, (1-2), 49-58.

44. Navrotsky, A.; Hon, R.; Weill, D. F.; Henry, D. J., Thermochemistry of glasses and liquids in the systems CAMGSI2O6-CAAL2SI2O8-NAALSI3O8, SIO2-CAAL2SI2O8-NAALSI3O8 and SIO2-AL2O3-CAO-NA2O. *Geochimica Et Cosmochimica Acta* **1980,** *44*, (10), 1409–1423.

45. Navrotsky, A.; Tian, Z-R. Systematics in the Enthalpies of Formation of Anhydrous Aluminosilicate Zeolites, Glasses, and Dense Phases, *Chemistry - A European Journal* **2001**, *7*, (4). 769-774

46. Robie, R.; Hemingway, B., *Thermodynamic properties of minerals and related substances at 298.15 K and 1 bar (10^5 pascals) pressure and at higher temperatures*. US Geological Survey Bulletin: Denver, Colorado, 1995; p 461.

47. Glushko, V.; Medvedev, V.; Bergman, G.; Vasilev, B. P.; Gurvich, L. V.; Alekseev, V. I.; Kolesov, V. P.; Yungman, V. S.; Ioffe, N.; Vorabev, A. F.; Reznitskii, L. A.; Khodakovskii, I. L.; Smirnova, N. L.; Galchenko, G.; Baibuz, V. F., Thermicheskie konstanti veshtestv. *Academy of Science, Moscow, U.S.S.R* **1972**.

48. Bale, C. W.; Belisle, E.; Chartrand, P.; Decterov, S. A.; Eriksson, G.; Hack, K.; Jung, I.-H.; Kang, Y.-B.; Melancon, J.; Pelton, A. D.; Robelin, C.; Petersen, S., FactSage thermochemical software and databases - recent developments. *Calphad* **2009,** *33*, (2), 295-311.

49. Fialips, C.-I.; Navrotsky, A.; Petit, S., Crystal properties and energetics of synthetic kaolinite. *American Mineralogist* **2001,** *86*, 304-311.

50. Kiseleva, I.; Navrotsky, A.; Belitsky, I.; Fursenko, B., Thermochemical study of calium zeolites—heulandite and stilbite. *American Mineralogist* **2001,** *86*, 448-455.

51. Kiseleva, I.; Navrotsky, A.; Belitsky, I.; Fursenko, B., Thermochemistry and phase equilibria in calcium zeolites. *American Mineralogist* **1996,** *81*, 658-667.

52. Chai, L.; Navrotsky, A., Thermochemistry of carbonate-pyroxene equilibria. *Contributions to Mineralogy and Petrology* **1993,** *114*, 139-147.

53. Trofymluk, O.; Levchenko, A. A.; Tolbert, S. H.; Navrotsky, A., Energetics of Mesoporous Silica: Investigation into Pore Size and Symmetry. *Chemistry of Materials* **2005,** *17*, (14), 3772-3783.

54. Liu, Q.; Navrotsky, A.; Jove-Colon, C. F.; Bonhomme, F., Energetics of cancrinite: Effect of salt inclusion. *Microporous and Mesoporous Materials* **2007,** *98*, (1-3), 227-233.

55. Kurdakova, S. V.; Grishchenko, R. O.; Druzhinina, A. I.; Ogorodova, L. P., Thermodynamic properties of syntethic calcium-free carbonate cancrinite. *Phys. Chem. Miner.* **2014,** *41*, 75-83.